Absolute elastic differential electron scattering cross sections in the intermediate energy region. I. H_2*

Santosh K. Srivastava,† A. Chutjian, and S. Trajmar

Jet Propulsion Laboratory, California Institute of Technology, Pasadena, California 91103
(Received 5 March 1975)

A new method for measuring absolute electron-impact differential cross sections (DCS) for elastic scattering in gases is described. The technique uses a well-defined crossed-beam scattering geometry in which the relative target densities of an unknown and a secondary standard gas are accurately determined by a calibrated flowmeter and a pressure gauge. The method is applied to the measurement of elastic scattering from H_2 (which, in the present work, also includes rotational excitation) relative to elastic scattering from He, the secondary standard. The relative DCS for H_2 are then placed on the absolute scale by using recently measured absolute elastic DCS for He. Measurements for H_2 are reported at incident electron energies of 3–75 eV, and in the angular range 20°–135°. Differential and integral cross sections at each energy are compared with previous measurements and recent theoretical calculations.

I. INTRODUCTION

Electron impact excitation cross sections are of importance in a number of fields (plasma, laser, ionospheric physics, radiation chemistry, etc.). Although these cross sections can, in principle, be calculated theoretically, accurate prediction is possible only either at high electron impact energies where plane wave theories are applicable, or at low energies where there are only a small number of open channels for excitations. At intermediate electron impact energies, i.e., in the region between 1 and 100 eV, although formal theoretical methods are available, they are not practical for accurate cross section calculations for other than the lightest elements. The situation is not much better from the experimental point of view either. At high energies (above 100 eV) Bromberg[1] has obtained absolute cross sections for a number of gases by determining all quantities that relate the experimentally measured scattering intensities to the corresponding cross sections. At energies below 100 eV accurate absolute values exist only for atomic hydrogen and helium.[2–4] With recent advances in laboratory techniques the determination of relative scattering intensities has been carried out in a number of laboratories, but the problem of measurements of absolute cross sections or the normalization of relative measurements to the absolute scale is still not satisfactorily solved.

Experimental difficulties associated with the determination of absolute cross sections, or the normalization of cross sections to the absolute scale by indirect methods, depend on the method used. Even for crossed-beam scattering experiments the scattering geometry changes considerably with scattering angle (see Ref. 5 for a detailed discussion), the transmission function of the electron optics is usually quite difficult to obtain, and the density (flux and velocity distributions) of the target beam particles is not well known. However, due to some recent developments, it is now possible to overcome the above difficulties and obtain accurate absolute values of elastic differential cross sections using the crossed-beam scattering arrangement. These developments are (a) a fairly accurate knowledge of He elastic differential cross sections,[2–4] and (b) availability of reliable theoretical expressions[6–12] for the flux and velocity distributions of the target beam particles.

In the present paper we describe a calibration method which utilizes these new developments for measuring the *ratio* of the elastic differential cross section (DCS) of H_2 to that of He. A well-defined crossed-beam geometry is used in which the relative target densities of H_2 and He are accurately determined by calibrated flow meters. The absolute values of the H_2 DCS are obtained by multiplying these ratios by the helium DCS, thus using He as a secondary standard. An important result of these measurements is the fact that once absolute *elastic* DCS's are available, absolute *inelastic* cross sections can be easily obtained by measuring inelastic-to-elastic scattering intensity ratios.

In Sec. II we present the basic principles of the relative flow-rate technique used. The electron-scattering spectrometer and the method of data acquisition are described in Sec. III. In Sec. IV, results are presented, and elastic H_2 DCS and integral cross sections are compared to previous experimental results and to recent predictions of several theories.

II. THEORY

In a crossed-beam scattering arrangement, a target beam is produced by flowing a gas through either a fine hole, or capillary tube, or array. A monoenergetic electron beam obtained from an electron monochromator is made to cross this molecular beam at 90°. Electrons collide with the molecule of the target beam and are consequently scattered in all directions. The experimental measurements consist of determining the energy and angular distribution of these scattered electrons as a function of impact energy. A schematic diagram of such a crossed-beam scattering arrangement is shown in Fig. 1.

The quantity obtained experimentally is the number of electrons/sec of a particular energy that is scattered into an angle θ with respect to the incident electron beam. The quantity of interest is the differential cross section $\sigma(\theta)$ for this process. A relation between these two quantities has been derived by several authors in the past.[11,13–15] For the sake of clarity in the following, we shall rederive this relation. Figure 2 shows a magnified

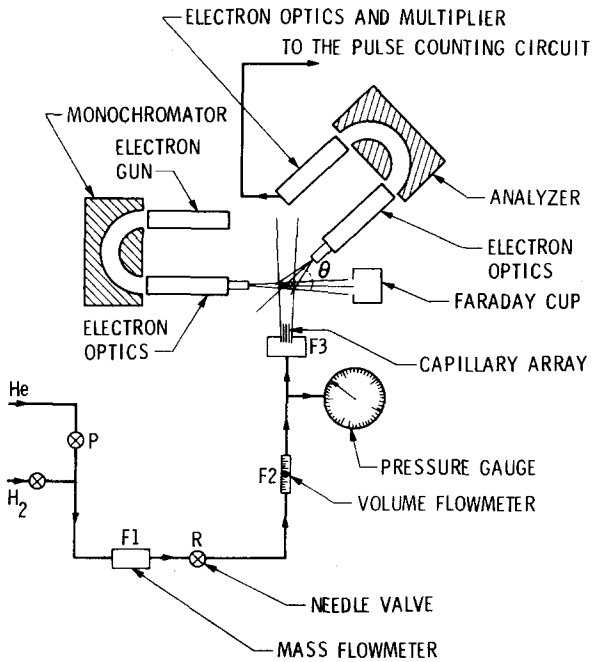

FIG. 1. Schematic diagram showing the gas flow system and the arrangement of electron optics.

view of the interaction region. Suppose the electron beam travels in the x direction and the molecule beam in the z direction. Also, suppose that the electron beam is monoenergetic and the velocities of molecules in the molecular beam are negligible compared to the velocity of electrons. Each volume element within the interaction region will scatter electrons. Assuming only single scattering, the number of detected electrons/sec scattered by a volume element $d\tau = dx\,dy\,dz$ into the differential solid angle $d\Omega(x, y, z)$ at an angle θ is given by

$$d\dot{N}_e(x, y, z) = K\sigma'[\theta(x, y, z)]F_e(x, y, z)n_b(x, y, z)d\Omega(x, y, z)d\tau\ , \quad (1)$$

where $\sigma'[\theta(x, y, z)]$ is the DCS in units of area/sr; $F_e(x, y, z)$ is the flux of electrons, i.e., number of electrons/sec crossing a unit area located at $d\tau$; $n_b(x, y, z)$ is the density of molecules in $d\tau$; and K is the transmission efficiency of the analyzer–detector system. In Eq. (1) we have used the most general notation wherein *all* the quantities in the integrand may depend on the (x, y, z) location of the scattering volume element $d\tau$ (see Fig. 2). For example, $\sigma'[\theta(x, y, z)]$ is the DCS for scattering from the element $d\tau$ at location (x, y, z), where $d\tau$ subtends an angle θ at the analyzer as measured from the incident electron beam direction.

The number of electrons/sec, $\dot{N}_e$, scattered and detected at angle θ by the entire interaction volume V and solid angle of acceptance Ω is obtained by integrating Eq. (1),

$$\dot{N}_e = K\int_V\int_\Omega \sigma'[\theta(x, y, z)]F_e(x, y, z)n_b(x, y, z)\,d\Omega\,d\tau. \quad (2)$$

In the most general case, the cross section $\sigma'[\theta(x,y,z)]$ could vary significantly with θ even within the small range of θ associated with the solid angle of acceptance Ω of the analyzer. Equation (2) is a relation between the experimentally-observed scattered signal at an angle θ and the corresponding cross section. The required cross section is obtained formally by inverting the integral equation [Eq. (2)]. In practice, this could be done by choosing a reasonable cross-section function as a first guess, and refining this choice through an iterative procedure. For the present purposes, it is sufficient to assume that some average cross section $\sigma(\theta)$ may be used over the entire volume element V and solid angle Ω, so that Eq. (2) may be written as

$$\dot{N}_e = K\sigma(\theta)\int_V\int_\Omega F_e(x, y, z)n_b(x, y, z)\,d\Omega\,d\tau\ . \quad (3)$$

If the average speed of the molecules in the beam is denoted by $\bar{v}_b$, then $n_b(x, y, z) = F_b(x, y, z)/\bar{v}_b$, where $F_b(x, y, z)$ is the flux in number of atoms (molecules)/sec crossing unit area located at $d\tau$. Thus, rewriting Eq. (3), one obtains

$$\dot{N}_e = K\sigma(\theta)\frac{1}{\bar{v}_b}\int_V\int_\Omega F_e(x, y, z)F_b(x, y, z)\,d\Omega\,d\tau\ . \quad (4)$$

We shall hereafter denote the double integral in Eq. (4) as β, the "overlap integral," since it represents the extent of coverage between the electron and target beams within V and Ω.

We see from Eq. (4) that in order to obtain an absolute value of $\sigma(\theta)$ one has to obtain the absolute values of K, β, and $\bar{v}_b$. Experimentally, such a determination at low and intermediate electron energies is very difficult and may involve large errors. Rather, one can perform a relative measurement by measuring the number of scattered electrons for two different target molecules $(\dot{N}_e)_1$ and $(\dot{N}_e)_2$ in such a way that the incident electron beam, the detector efficiency, and the scattering geometry do not change during the time of measurement.

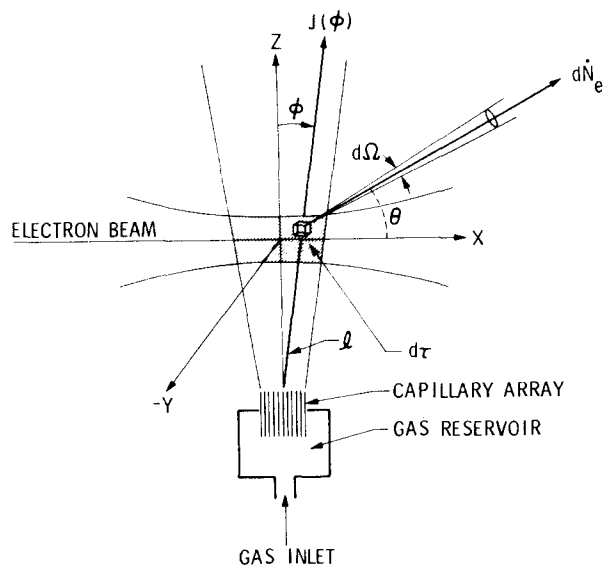

FIG. 2. A magnified view of the interaction region. $J(\phi)$ is the flux in molecules $\text{sec}^{-1}\text{-sr}^{-1}$ at polar angle ϕ. $d\dot{N}_e$ represents the number of electrons per second elastically-scattered into a solid angle $d\Omega$ at an angle θ with respect to the incident electron beam direction.

Thus, K, Ω, $F_e(x, y, z)$ will remain the same for both gases, and the ratio of the two counting rates will be given by the relation

$$(\dot{N}_e)_1/(\dot{N}_e)_2 = [\sigma_1(\theta)/\sigma_2(\theta)]\,[(\bar{v}_b)_2/(\bar{v}_b)_1]\,[\beta_1/\beta_2]\,, \tag{5}$$

or

$$\sigma_1(\theta)/\sigma_2(\theta) = [(\dot{N}_e)_1/(\dot{N}_e)_2]\,[(\bar{v}_b)_1/(\bar{v}_b)_2]\,[\beta_2/\beta_1]\,. \tag{6}$$

In order to obtain this ratio, expressions are needed for the average speed of molecules in the beam and for the flux $F_b(x, y, z)$ at various points within the interaction volume V. For a molecular beam formed by a single capillary tube within an array, these expressions have been derived and experimentally verified by Olander *et al.*[6-8,10] Although we use a capillary array for generating the target beam, the single tube distributions lead to the same conclusions and will be used here for simplicity of discussion. According to Olander *et al.*,[6-8,10] the angular flux distribution of molecules leaving one of the tubes of the capillary array is given by

$$J(\phi) = (\nu_s/\pi)\,(\pi a^2)\,j(\phi)\,, \tag{7}$$

where $J(\phi)$ is flux in molecules $\text{sec}^{-1} \cdot \text{sr}^{-1}$ at a polar angle ϕ from the tube axis (Fig. 2), ν_s the rate at which molecules in the gas reservoir enter a unit area of the capillary tube, a the radius of the tube, and $j(\phi)$ defines a distribution function for the molecular flux in the beam. At a point $d\tau$ (Fig. 2) within the interaction volume, the molecular flux due to a tube of the capillary array crossing a unit area per second is $J(\phi)/l^2$ where l is the distance of the volume element $d\tau$ from the tube. The total flux $F_b(x, y, z)$ crossing a unit area per second at this volume element will be a sum of contributions from each tube of the array and can be expressed as some factor B times the flux of one tube,

$$F_b(x, y, z) = BJ(\phi)/l^2 = B(\nu_s/\pi)\,(\pi a^2)\,j(\phi)/l^2\,. \tag{8}$$

In Eq. (8) factors B, a, l, and $j(\phi)$ are purely functions of the geometry of the capillary array and do not depend upon the type of gas. Therefore, for the two gases, No. 1 and No. 2, the ratio β_2/β_1 in Eq. (6) is given by

$$\beta_2/\beta_1 = \nu_{s2}/\nu_{s1}\,, \tag{9}$$

where ν_s has been defined before and is related to the total flow rate $\dot{N}_b$ of the gas passing through the capillary array by

$$\dot{N}_b = K_p \nu_s A\,, \tag{10}$$

where K_p is the transmission probability (or Clausing factor) of the capillary array, and A its total open area. Both K_p and A depend only on the geometry of the capillary array and thus cancel in the ratio of Eq. (9), giving

$$\beta_2/\beta_1 = \dot{N}_{b2}/\dot{N}_{b1}\,. \tag{11}$$

Olander *et al.*[8] have also derived an expression for the average velocity $\bar{v}_b$ of the beam particles as

$$\bar{v}_b = \alpha\left[\int_0^\infty z^3 f(z)\,dz \Big/ \int_0^\infty z f(z)\,dz\right]^{1/2}\,, \tag{12}$$

where $\alpha = (2kT/m)^{1/2}$ is the most probable speed of a gas having a Maxwellian distribution of speeds at the source temperature T, m the molecular weight of the gas particles, k the Boltzmann constant, z the reduced speed of molecules given by v/α with v as the speed of a molecule in the beam, and $f(z)$ the normalized number density speed distribution of the centerline beam. Using Eq. (12), the ratio $(\bar{v}_b)_1/(\bar{v}_b)_2$ needed in Eq. (6) is

$$(\bar{v}_b)_1/(\bar{v}_b)_2 = [m_2/m_1]^{1/2}\,, \tag{13}$$

where we have assumed that the temperature in the gas reservoir (Fig. 2) for the two gases is the same.

Substituting Eqs. (11) and (13) in Eq. (6) we get

$$\sigma_1(\theta)/\sigma_2(\theta) = [(\dot{N}_e)_1/(\dot{N}_e)_2]\,[m_2/m_1]^{1/2}\,[\dot{N}_{b2}/\dot{N}_{b1}]\,. \tag{14}$$

Equations (7), (10), and (12) are applicable only under certain conditions. The pressure in the gas reservoir (Fig. 2) should be low enough so that the total flow of gas through the capillary array will not be hydrodynamic, that is

$$K_{nD} = \lambda/D \geq 1\,, \tag{15}$$

where K_{nD} is the Knudsen number, D the diameter of the tube, and λ the mean free path of the molecules in the gas reservoir. When these conditions are fulfilled, then the total gas flow rate $\dot{N}_b$ through the capillary array is directly proportional to the pressure in the gas reservoir and Eq. (14) can be written in the form

$$\sigma_1(\theta)/\sigma_2(\theta) = [(\dot{N}_e)_1/(\dot{N}_e)_2]\,[p_2/p_1]\,, \tag{16}$$

where p_1 and p_2 are the pressurs of gas No. 1 and gas No. 2 in the gas reservoir.

III. MEASUREMENT OF THE DIFFERENTIAL CROSS SECTIONS

A. Apparatus

A schematic diagram of the apparatus used is shown in Fig. 1. The electron source, optics, energy analyzers, and detector have been described earlier,[16] and only a brief general description will be given here. The gas-flow system is important from the point of view of the absolute cross-section determination and will be described in some detail.

An energy-selected electron beam (~60 meV full width at half-maximum, FWHM) of 5 to 10 nA current is focussed onto the target molecular beam. The scattered electrons are collected over a small solid angle ($\sim 10^{-3}$ sr), energy-analyzed, and detected by an electron multiplier.

The molecular beam is produced by flowing the gas under study through a capillary array. This array is made up of a number of fine holes in a nonmagnetic stainless steel cylinder. This cylinder is 0.51 cm long and of overall diameter 0.64 cm, of which only an unmasked portion of 0.11 cm diameter is used. The diameter of a hole in the cylinder is 5.1×10^{-3} cm. The mechanical arrangement is such that the capillary array and the electron energy analyzer are fixed, while the electron gun is rotatable about the scattering volume

TABLE I. H_2 differential elastic cross sections $\sigma(E_0\theta)$ (10^{-20}m^2/sr). In brackets are the ratios σ_{H_2}/σ_{He}.

θ (deg) \ E_0 (eV)	3	5	7	10	15	20	30	40	60	75
20	1.14 (6.43)	1.87 (8.21)	2.02 (7.09)	1.74 (5.34)	1.66 (4.41)	1.19 (3.22)	0.85 (2.17)	0.76 (2.03)	0.59 (1.66)	0.49 (1.53)
30	1.06 (5.28)	1.68 (6.95)	1.72 (6.14)	1.50 (4.82)	1.36 (3.94)	0.92 (2.79)	0.61 (1.86)	0.47 (1.57)	0.36 (1.32)	0.23 (1.06)
40	0.92 (4.27)	1.34 (5.58)	1.30 (5.04)	1.18 (4.13)	1.03 (3.21)	0.68 (2.37)	0.40 (1.54)	0.30 (1.29)	0.22 (1.08)	0.13 (0.83)
50	0.79 (3.47)	1.09 (4.61)	1.13 (4.55)	1.00 (3.70)	0.72 (2.76)	0.52 (2.08)	0.29 (1.32)	0.19 (1.06)	0.13 (0.89)	0.07 (0.65)
70	0.63 (2.33)	0.73 (2.75)	0.62 (2.54)	0.59 (2.36)	0.36 (1.63)	0.25 (1.35)	0.14 (0.84)	0.078 (0.71)	0.048 (0.56)	0.024 (0.45)
90	0.64 (1.94)	0.54 (1.82)	0.46 (1.66)	0.36 (1.34)	0.23 (0.98)	0.15 (0.74)	0.071 (0.55)	0.040 (0.47)	0.023 (0.42)	0.012 (0.38)
115	0.88 (1.99)	0.64 (1.53)	0.45 (1.13)	0.29 (0.76)	0.15 (0.45)	0.092 (0.38)	0.042 (0.31)	0.024 (0.30)	0.018 (0.34)	0.009 (0.38)
135	1.29 (2.18)	0.90 (1.57)	0.59 (1.08)	0.34 (0.63)	0.16 (0.39)	0.092 (0.29)	0.044 (0.23)	0.022 (0.27)	0.022 (0.34)	0.009 (0.37)
Integral (10^{-20} m^2)	11.2	11.1	9.38	7.68	5.54	3.73	2.24	1.66	1.26	0.86
Momentum transfer (10^{-20} m^2)	12.3	10.1	7.35	5.31	3.04	1.92	1.00	0.59	0.45	0.22

over the angular range $-30°$ to $+136°$. The energy of the incident electron beam was calibrated by using the 19.3 eV resonance in helium. The true zero scattering angle was determined from the symmetry about that zero of the scattering intensity corresponding to the 2^1P excitation in He.

The gas-flow system consists of the He and H_2 lines, valves, flowmeters, and pressure gauge, as indicated in Fig. 1. The desired gas flows through a mass flowmeter F1. This meter measures the number of standard cubic centimeters that flow through it per minute. It consists of an electrically heated tube and an arrangement of thermocouples to measure the differential cooling caused by a gas passing through the tube. The design is such that the measured flow rate depends on neither pressure nor temperature changes of the gas. The flow rate of the gas is controlled by a fine needle valve R across which the pressure drops from about 250 to 10 Torr. In order to check the accuracy and consistency of the mass flowmeter, we installed a second flowmeter F2 which essentially measures the volume flow rate of the gas. The measurement of volume flow by this meter depends on the temperature as well as the pressure of the gas on either side of the flowmeter. The pressure of the gas in the reservoir F3 is measured by a calibrated pressure gauge.

B. Method

In order to obtain the absolute values of cross sections, either Eq. (14) or Eq. (16) is used. These equations are valid only if the condition given by Eq. (15) is fulfilled. This condition will be satisfied if the pressure of the gas in chamber F3 (Fig. 1) is proportional to its flow rate through the capillary array. Therefore, we first determine the curve representing the relationship between the flow rate and the pressure p. In addition to this, we draw a pressure dependence curve for the scattered intensity. In actual measurements the pressure in the chamber F3 is adjusted to some value which lies in the linear region of these two curves. The following steps are then taken to obtain the quantities needed in Eq. (14) or Eq. (16): (a) H_2 is flowed through the system to form the target beam and the rate, $\dot{N}_e(H_2)$, of elastically scattered electrons is recorded. At the same time the pressure p and flow rate $\dot{N}_b(H_2)$ of H_2 are also obtained. (b) The flow of H_2 is then stopped and the system is pumped out to about 1×10^{-7} Torr pressure which takes about 15 min. The He is let in and the elastic scattering rate $\dot{N}_e$(He), pressure p, and the flow rate $\dot{N}_b$(He) are obtained.

In both these operations the elastic scattering is ob-

TABLE II. Various sources of errors that contribute to the total error in the measurement of the ratio σ_{H_2}/σ_{He}.

1. (a) Error in the ratio of flow rates $\dot{N}_{b_2}/\dot{N}_{b_1}$ [Eq. (14)].	±5%
or	
(b) Error in the ratio of measured pressures p_2/p_1 [Eq. (16)]	±5%
2. Estimated error in the ratio $(\dot{N}_e)_1/(\dot{N}_e)_2$ [Eq. (16)].	±2%
3. Estimated error due to the change in the incident electron beam current.	±3%
Total	±10%

tained by the method of multichannel scaling, and the intensities are obtained by integrating the area under the respective elastic features. These measured elastic scattering intensities at an angle θ consist of two components. One is due to scattering from the molecular beam where the pressure is estimated to be about 10^{-3} Torr and the other is contributed by the background gas at a pressure of about 10^{-6} Torr. In order to estimate the magnitude of the background scattering, we provided an alternate gas leak to the vacuum chamber. The flow to the chamber was switched from the capillary array to the alternate gas inlet, and the proper background pressure for the desired gas was established. At an impact energy E_0, the angular distribution of elastically scattered electrons was then measured. It was found that for both He and H_2, above 20° scattering angle, the background scattering was between 1% to 2% of the scattering from the beam formed by the capillary array. Therefore, in the ratio of scattered intensities of H_2 to He, the error caused by the background scattering can be neglected in comparison with other sources of error. In the present apparatus, the electron gun, optics, energy analyzers and electron multiplier are differentially pumped. Therefore, in replacing H_2 by He the properties of the system are not affected. This was evidenced by the fact that the incident electron beam current as measured by a Faraday cup was constant to ± 3% during the whole operation.

We obtain by this method primarily the angular distribution of ratios of elastic H_2 DCS to that of He. These ratios are then multiplied by absolute He cross sections in order to get absolute H_2 DCS. As our choice of values for the He DCS, we use recent measurements of McConkey and Preston.[4] In their paper they summarize previous helium elastic cross section measurements and compare them with their results. We chose their cross sections because they represent the most recent experimental measurements over the whole energy range considered here. However, at each electron impact energy, they cover only an angular range of 20° to 90°. In order to obtain values of elastic He DCS at scattering angles above 90°, we extrapolated the results of McConkey and Preston in such a way that the angular distribution curve followed the shape of the theoretical curve calculated by Labahn and Callaway.[3] We emphasize that the primary results of the present measurements are the *ratios* of the H_2 DCS to that of helium. The absolute values of the H_2 DCS can be renormalized should more accurate He cross sections become available in the future.

The resolution of 60 meV FWHM in the present work was not sufficient to resolve rotational transitions in H_2, so that the present elastic DCS measurements also in-

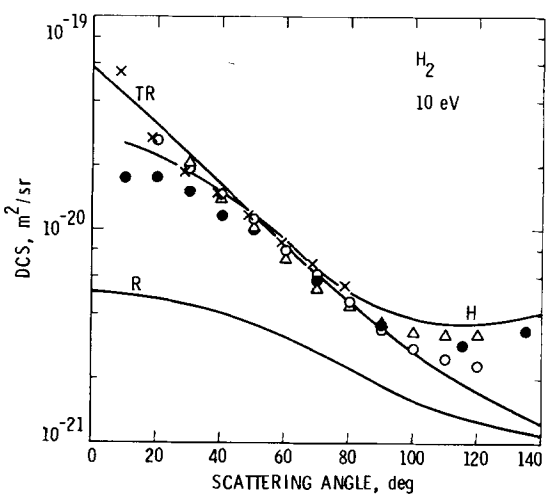

FIG. 3. Elastic DCS at 10 eV. ●, present measurements. o, Linder and Schmidt.[20] ×, Trajmar *et al.*[18] Δ, Bullard and Massey,[19] normalized to present results at 90°. TR, theoretical calculations of Truhlar and Rice,[22] H, that of Hara,[21] and R, that of Rozsnyai.[23]

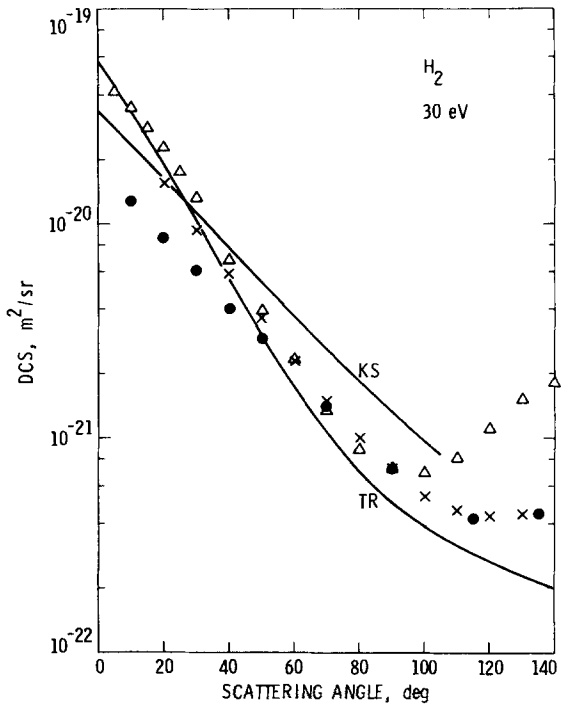

FIG. 4. Elastic DCS at 30 eV. ●, present measurements. Δ, Webb,[25] normalized to present results at 90°. ×, Williams,[24] normalized to present results at 90°. TR and KS represent theoretical calculations of Truhlar and Rice,[22] and Khare and Shobha,[26] respectively.

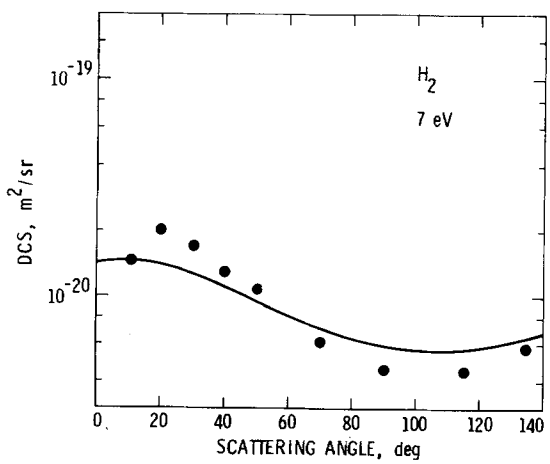

FIG. 5. Elastic DCS at 7 eV. ●, present measurements. The solid line represents calculations of Rescigno *et al.*[27]

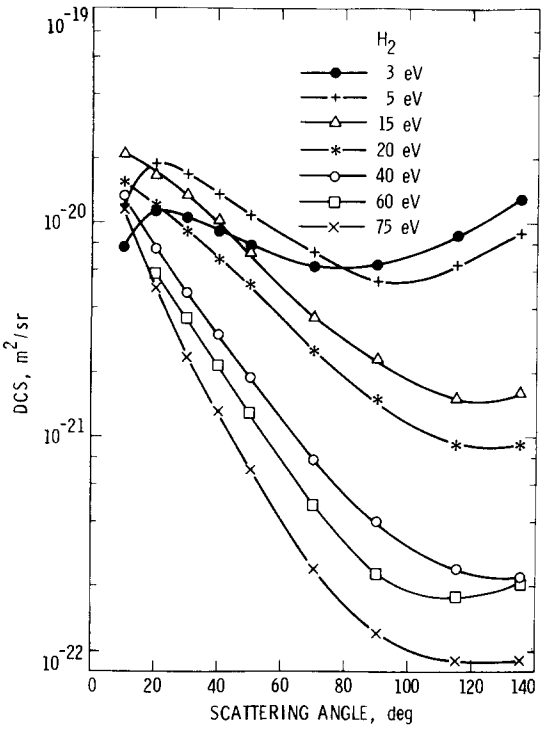

FIG. 6. Elastic DCS at 3, 5, 15, 20, 40, 60, and 75 eV. Symbols represent results of present measurements. Solid lines are interpolations between these symbols.

clude these transitions. Absolute rotational–excitation cross sections will be presented in a future publication.[17]

IV. RESULTS AND DISCUSSION

Using the method described above the ratios of H_2 DCS to that of He at incident energies E_0 of 3, 5, 7, 10, 15, 20, 30, 40, 60, and 75 eV were obtained. At each energy the angular range extended from 20° to 135°. In these measurements the energy resolution of the spectrometer was about 60 meV. As noted earlier, scattered electrons with energy loss corresponding to rotational excitations in H_2 were not resolved from the elastically-scattered electrons. Thus, the H_2 DCS reported here are a sum of elastic and rotational cross sections.

Table I gives the results of the present measurements. In brackets are the ratios of H_2 DCS to that of He. From these the absolute values of H_2 DCS have been calculated and are given in the same table. Below 20° and above 135° the angular distributions were extrapolated. These were then used for the calculation of integral and momentum-transfer cross sections which are shown in Table I at the bottom of each column.

At each energy and at each angle at least five sets of data were obtained for the ratio of the two differential cross sections. The data were reproducible within ± 5%. However, the estimated error for these ratios is about ± 10%. In Table II we summarize various sources of errors that contribute to the total error mentioned above. The error in the absolute differential cross sections has been estimated to be about ± 15% which is the root-mean-square of a ± 10% error in the ratio measurements and a ± 12% error of McConkey and Preston.[4] The error associated with the integral cross sections is estimated to be ± 18% and with the momentum-transfer cross sections to be ± 20%. These errors are a sum of errors contributed by individual differential cross sections and errors in the extrapolations employed below 20° and above 135°.

Figures 3–6 show the angular dependence of the elastic DCS at different impact energies. In Figs. 3 and 4 we have compared our measurements with several previous experimental and theoretical results. A review of all the previous experimental measurements and theoretical calculations has been provided by Trajmar *et al.*[18] For present purposes, in order to avoid confusion in the figures due to the presence of many symbols, we show only some pre-1970 experimental data, but all readily available experimental measurements published after 1970. At the same time, the present results have been compared only with those theories whose predictions are close to experimental data. Furthermore, these last comparisons have been made only at 10 and 30 eV.

In Fig. 3 we have compared our elastic DCS with experimental results of Bullard and Massey,[19] Linder and Schmidt,[20] and Trajmar *et al.*[18] All experimental data included rotational excitation except that of Linder and Schmidt. Data of Bullard and Massey, in arbitrary units, were normalized to our values at 90°. Within the limits of experimental errors there is a good agreement between various measurements at angles above 40°. At angles below 40° our values are considerably lower than the results of other measurements. This discrepancy may be due to an insufficient effective path-length correction in these measurements. If this correction is not applied then the values of measured cross sections tend to increase at low angles. Bullard and Massey did not apply such a correction. Trajmar *et al.*[18] estimated this correction factor. Linder and Schmidt calibrated their instrument by using helium cross sections of Andrick and Bitsch[2] which in effect provided the effective

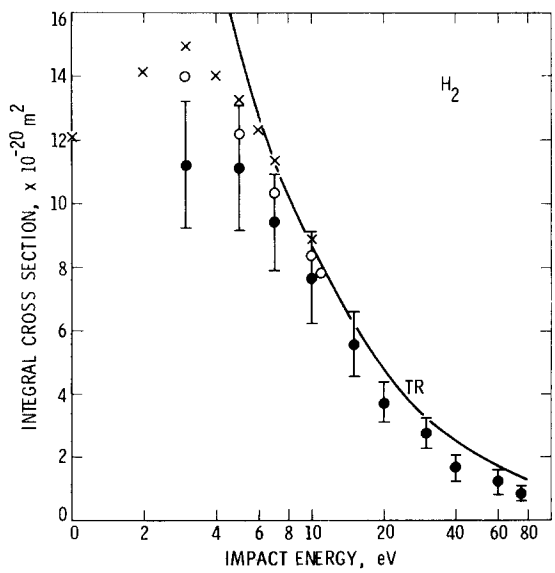

FIG. 7. Integral cross sections. ●, present measurements. Error bars represent ±18% error. o, Linder and Schmidt.[20] ×, Golden *et al.*[28] TR represents theoretical calculations of Truhlar and Rice.[22]

path-length correction. In our measurements, we have utilized recent experimental helium DCS of McConkey and Preston.[4] Therefore, the differences between our measurements and of Linder and Schmidt reflect the different helium cross section values.[2,4] It is found that the use of helium cross sections of Andrick and Bitsch rather than those of McConkey and Preston gives better agreement between the present results and those of Linder and Schmidt.

Theoretical predictions for differential elastic cross sections at 10 eV are shown by solid lines in Fig. 3. The curve labeled H refers to the calculations of Hara,[21] while the curve referred to as TR gives the polarized Born approximation results of Truhlar and Rice.[22] This latter theory is in good agreement with our results between 40° and 90°, but below 40° and above 90° the differences between the two results are rather large. The curve marked R represents the Born calculations of Rozsnyai[23] which neglect exchange and polarization and use Heitler–London-like wavefunctions. We find that these calculations give an angular distribution which is similar in shape to the angular distribution of the present work, but the absolute magnitudes of calculated cross sections are too low.

In Fig. 4 we present our differential elastic cross sections along with some experimental and theoretical results at 30 eV. There is only one recent experimental measurement by Williams[24] at this energy. We find that our measurements are in good agreement with his results above 40°, but below 40° the agreement is rather poor. This discrepancy may again be due to inadequate volume correction at these low angles. The other experimental angular distribution at this energy is due to Webb[25] and was given in arbitrary units. We have normalized his results to our results at 90°. Here again, the agreement is good between 50° and 90° but at other angles the differences are large. Webb did not apply a volume correction. At this energy there are two theoretical calculations whose results are readily available and are shown by solid curves marked TR and KS. The TR curve is the result of polarized Born-approximation calculations by Truhlar and Rice.[22] The KS curve represents recent calculations of Khare and Shobha[26] (denoted by curve A in Fig. 3 of their paper). They employed the plane-wave approximation with a semiempirical potential and one-center wave functions. We find that the angular distribution given by their calculations is similar to our results but the magnitude of each cross section is higher than ours.

In Fig. 5 results of our measurements at 7 eV electron impact energy are compared with recent calculations of Rescigno *et al.*[27] These cross sections were obtained from approximate solutions of the Lippmann–Schwinger equations. Within limits of experimental error the agreement is quite good.

In Fig. 6 we show plots of angular distributions obtained in the present work at the indicated energies. These plots are given for the sake of showing shapes and magnitudes of the angular distribution curves.

In Fig. 7 we present our integral cross sections along with experimental results of Linder and Schmidt[20] and Golden *et al.*,[28] and theoretical calculations of Truhlar and Rice.[22] Within the error limit of the present measurements (± 18%) our results are in agreement with previous data shown in Fig. 7.

ACKNOWLEDGMENTS

We are grateful to Dr. T. N. Rescigno, Mr. C. W. McCurdy, and Professor V. McKoy for results of their theoretical calculations prior to publication.

*Supported by the National Aeronautics and Space Administration under Contract No. NAS7-100 to the Jet Propulsion Laboratory.

†NRC-NASA Resident Research Associate.

[1]J. P. Bromberg, J. Chem. Phys. 50, 3906 (1969).
[2]D. Andrick and A. Bitsch, *Abstracts of the* VII *International Conference on the Physics of Electronic Atomic Collisions* (North Holland, Amsterdam, 1971), p. 87. Also, J. Phys. B 8, 393 (1975).
[3]R. W. Labahn and J. Callaway, Phys. Rev. A 2, 366 (1970).
[4]J. W. McConkey and J. A. Preston, J. Phys. B 8, 63 (1975).
[5]R. T. Brinkmann, S. Trajmar, and R. Brewington (to be published).
[6]D. R. Olander and V. Kruger, J. Appl. Phys. 41, 2769 (1970).
[7]D. R. Olander, J. Appl. Phys. 40, 4650 (1969).
[8]D. R. Olander, R. H. Jones, and W. J. Siekhaus, J. Appl. Phys. 41, 4388 (1970).
[9]J. A. Giordmaine and T. C. Wang, J. Appl. Phys. 31, 463 (1960).
[10]R. H. Jones, D. R. Olander, and V. R. Kruger, J. Appl. Phys. 40, 4641 (1969).
[11]G. C. Angel and R. A. Giles, J. Phys. B 5, 80 (1972).
[12]J. C. Johnson, A. T. Stair, and J. L. Pritchard, J. Appl. Phys. 37, 1551 (1966).
[13]J. Kessler and D. Weichert, Z. Phys. 212, 48 (1968).
[14]B. Bederson, *Methods of Experimental Physics*, Vol. 7, Part A (Academic, New York, 1968), p. 67.
[15]J. W. Hooper, W. C. Lineberger, and F. M. Bacon, Phys. Rev. 141, 165 (1966).
[16]A. Chutjian, J. Chem. Phys. 61, 4279 (1974).
[17]S. K. Srivastava, R. I. Hall, S. Trajmar, and A. Chutjian, Phys. Rev. A (to be published).
[18]S. Trajmar, D. G. Truhlar, and J. K. Rice, J. Chem. Phys. 52, 4502 (1970).
[19]E. C. Bullard and H. S. W. Massey, Proc. R. Soc. A 133, 637 (1931).
[20]F. Linder and H. Schmidt, Z. Naturforsch. A 26, 1603 (1971).
[21]S. Hara, J. Phys. Soc. Jap. 22, 710 (1967).
[22]D. G. Truhlar and J. K. Rice, J. Chem. Phys. 52, 4480 (1970).
[23]B. R. Rozsnyai, J. Chem. Phys. 47, 4102 (1967).
[24]K. G. Williams, *Abstracts of the* VI *International Conference on the Physics of Electronic Atomic Collisions* (MIT Press, Boston, 1969), p. 735.
[25]C. M. Webb, Phys. Rev. 47, 384 (1935).
[26]S. P. Khare and P. Shobha, J. Phys. B 7, 420 (1974).
[27]T. N. Rescigno, C. W. McCurdy, Jr., and V. McKoy, Phys. Rev. A 11, 825 (1975).
[28]D. E. Golden, H. W. Bandel, and J. A. Salerno, Phys. Rev. 146, 40 (1966).